

Title	Interaction study of nitrogen ion beam with silicon
Author(s)	Schmidt, Marek E.; Zhang, Xiaobin; Oshima, Yoshifumi; Anh, Le The; Yasaka, Anto; Kanzaki, Teruhisa; Muruganathan, Manoharan; Akabori, Masashi; Shimoda, Tatsuya; Mizuta, Hiroshi
Citation	Journal of Vacuum Science & Technology B, 35(3): 03D101
Issue Date	2017-02-24
Type	Journal Article
Text version	publisher
URL	<a href="http://hdl.handle.net/10119/15365">http://hdl.handle.net/10119/15365</a>
Rights	Copyright 2017 American Vacuum Society. This article may be downloaded for personal use only. Any other use requires prior permission of the author and the American Vacuum Society. The following article appeared in Marek E. Schmidt, Xiaobin Zhang, Yoshifumi Oshima, Le The Anh, Anto Yasaka, Teruhisa Kanzaki, Manoharan Muruganathan, Masashi Akabori, Tatsuya Shimoda, Hiroshi Mizuta, Journal of Vacuum Science & Technology B, 35(3), 03D101- (2017) and may be found at <a href="http://dx.doi.org/10.1116/1.4977566">http://dx.doi.org/10.1116/1.4977566</a>
Description	

## Interaction study of nitrogen ion beam with silicon

Marek E. Schmidt,<sup>a)</sup> Xiaobin Zhang, Yoshifumi Oshima, and Le The Anh

*School of Materials Science, Japan Advanced Institute of Science and Technology, 1-1 Asahidai, Nomi 923-1292, Japan*

Anto Yasaka

*Hitachi High-Tech Science Corporation, 36-1 Takenoshita, Oyama-cho 410-1393, Japan and School of Materials Science, Japan Advanced Institute of Science and Technology, 1-1 Asahidai, Nomi 923-1292, Japan*

Teruhisa Kanzaki, Manoharan Muruganathan, Masashi Akabori, and Tatsuya Shimoda

*School of Materials Science, Japan Advanced Institute of Science and Technology, 1-1 Asahidai, Nomi 923-1292, Japan*

Hiroshi Mizuta

*School of Materials Science, Japan Advanced Institute of Science and Technology, 1-1 Asahidai, Nomi 923-1292, Japan; Nano Research Group, University of Southampton, Highfield, Southampton SO17 1BJ, United Kingdom; and Institute of Microengineering and Nanoelectronics, Universiti Kebangsaan Malaysia, UKM, 43600 Bangi, Selangor, Malaysia*

(Received 7 November 2016; accepted 9 February 2017; published 24 February 2017)

Focused ion beam technology with light gas ions has recently gained attention with the commercial helium and neon ion beam systems. These ions are atomic, and thus, the beam/sample interaction is well understood. In the case of the nitrogen ion beam, several questions remain due to the molecular nature of the source gas, and in particular, if and when the molecular bond is split. Here, the authors report a cross-sectional scanning transmission electron microscopy (STEM) study of irradiated single crystalline silicon by various doses and energies of nitrogen ionized in a gas field ion source. The shape and dimensions of the subsurface damage is compared to Monte Carlo simulations and show very good agreement with atomic nitrogen with half the initial energy. Thus, it is shown that the nitrogen molecule is ionized as such and splits upon impact and proceeds as two independent atoms with half of the total beam energy. This observation is substantiated by molecular dynamics calculations. High resolution STEM images show that the interface between amorphous and crystalline silicon is well defined to few tens of nanometers. © 2017 American Vacuum Society. [<http://dx.doi.org/10.1116/1.4977566>]

### I. INTRODUCTION

In the field of nanoelectronics and nano-electromechanical systems, resist based fabrication is established for mass fabrication. However, this process is relatively inflexible and often requires the preparation of a lithographic mask, which is both time consuming and requires a significant investment. Thus, prototyping techniques are commonly used to speed up the development and debugging of devices,<sup>1</sup> as well as repairing lithographic masks.<sup>2</sup> One such prototyping technique is the focused ion beam (FIB), where a beam of ions is generated, accelerated, and focused onto a sample in a very similar fashion to the scanning electron microscope. The beam is then used for milling or deposition of insulating or conducting layers. Until recently, Ga<sup>+</sup> FIB has been the dominant ion species. Stable ion sources offering a wide range of beam currents are well established. Beam spot sizes down to 3 nm are achieved; however, due to knock-on damage, the minimum achievable dimensions are typically larger.

The recent commercial integration of the gas field ion source (GFIS) into an ion microscope, offering helium<sup>3,4</sup> and neon beam,<sup>5</sup> has sparked a renaissance of the FIB technique

as device dimensions are further scaled toward the sub-10-nm range.<sup>6</sup> Aside from achieving higher resolution, some of the ions have added functionality. Hydrogen, for example, can integrate into the crystal structure of the target sample without causing disruptions,<sup>4</sup> which are currently limiting the application of He<sup>+</sup> GFIS-FIB.<sup>7</sup> Nitrogen, on the other hand, is used to create nitrogen-vacancy centers in diamond,<sup>8</sup> which function as quantum dots for future quantum computing.<sup>9</sup> Nitrogen has furthermore naturally a very high isotope purity, which has shown to be a problem for some other gas species such as neon; thus, a pure beam is expected.

Helium and neon both form atomic ions; therefore, its properties and interaction with matter can be understood from earlier experiments, and modeling using the SRIM/TRIM Monte Carlo (MC) simulation package<sup>10</sup> is well established. For experimental investigation of ion-induced damage, the observation of irradiated crystalline silicon by transmission electron microscopy (TEM) has shown to be most useful<sup>11–13</sup> due to the well-defined transition of silicon from crystalline to amorphous above a certain disorder threshold.<sup>14</sup> In the case of hydrogen, a recent report shows that, depending on the extraction field strength and tip shape, the species of the generated ions can be H<sup>+</sup>, H<sub>2</sub><sup>+</sup>, or H<sub>3</sub><sup>+</sup>.<sup>15</sup> The existence of the different ion species is directly evident from ghost images in secondary

<sup>a)</sup> Author to whom correspondence should be addressed; electronic mail: [schmidt@jaist.ac.jp](mailto:schmidt@jaist.ac.jp)

electron scans taken even without an imposed magnetic field. Nevertheless, a deeper understanding is required. Further investigation to understand all the implications of this property are expected in the future.

This ambiguity also applies to ionized nitrogen, which is the topic of this report. Nitrogen is very reactive in its atomic form ( $M \approx 14$  a.u.) and naturally occurs only in the form of  $N_2$ . The source gas in the nitrogen GFIS is therefore molecular nitrogen. The N–N bond is one of the strongest atomic bonds known in nature (binding energy: 9.79 eV, bond length: 0.11 nm). However, this is much smaller than the energies encountered in GFIS. Thus, it is not straight forward to predict what kind of ion will it form, and how will it interact with the sample. In fact, previously recorded mass spectra of electron ionized  $N_2$  gas have exhibited both  $N^+$  and  $N_2^+$  ions,<sup>16</sup> with ionization energies of  $24.21 \pm 0.25$  and  $15.54 \pm 0.25$  eV, respectively.<sup>17</sup> We therefore discuss two possible ionization and sample interaction mechanisms in this work as sketched in Figs. 1(a) and 1(b). The atomic configuration is shown after ionization and after impact with a crystalline silicon sample for 25 kV acceleration voltage. Note that ions are neutralized upon collision with an atomic surface.<sup>18</sup> Additionally, the expected interaction volume in crystalline silicon as obtained from TRIM simulations<sup>19</sup> and the depth profile of the nuclear stopping power per ion are shown. Nitrogen atoms can form nitrides with the target material after implantation.<sup>20,21</sup> However, this does not affect the ion trajectories while the kinetic energy of the

projectiles is significantly higher than the binding energy, and the formed nitrides remain amorphous unless annealed. The interaction between Si and N is, however, taken into account by the various simulation methods used in this work. In the first case [Fig. 1(a)], the breaking of the nitrogen molecule during ionization is considered. In that case, the beam is modeled in TRIM as N with 25 keV. The second discussed mechanism is depicted in Fig. 1(b), where the possibility of the molecule sustaining the ionization is shown. It then splits as it interacts with the target. Thus, the two resulting nitrogen atoms share the total energy, and are modeled as two atomic nitrogen with 12.5 keV. The variation of the energy ratio is neglected as it will not have any noticeable effect on the random process of ion–sample interactions. This approximation has been used for treating molecular nitrogen ions before.<sup>20</sup> The interaction volume is considerably shallower than the case depicted in Fig. 1(a), which is also manifested in the nuclear stopping power profiles. We also show the interaction volume for a beam energy of 16 keV for the second case, where the implantation depth is further reduced. It should be noted that TRIM yields independent results for each ion trajectory through an amorphous target based on the quantum mechanical treatment of the interatomic potential, and the dislocation and sputtering caused by previous ions are not taken into account for the next ion. Nevertheless, a good agreement between TRIM and experimental data has been shown for a large number of ions and targets,<sup>10</sup> and techniques to evaluate the accumulated damage have been proposed.<sup>11</sup> By evaluating the individual damage events from our TRIM simulations as function of depth, we have found very similar characteristics as the nuclear stopping power depth profiles in Fig. 1.

As can be understood from Fig. 1, depending on the ionization and interaction mechanism, the irradiated sample is very differently affected and should be clearly distinguishable from each other in cross section samples. To date, however, this has not yet been reported. In this work, we show experimental as well as molecular dynamics (MD) simulation results which clarify that the nitrogen GFIS-FIB follows the mechanism illustrated in Fig. 1(b), in agreement with common treatment of nitrogen ion beams in the field of nuclear science.<sup>20</sup> Based on these findings, we present a comparison of the nitrogen ion beam with other common ion beams.

## II. EXPERIMENTAL METHODS

### A. $N_2^+$ GFIS-FIB

The nitrogen beam was generated in the GFIS-FIB nanofabrication system developed by Hitachi High-Tech Science Corporation, comprising the atomically sharp emission tip that is cooled by a closed-cycle helium cryocooler.<sup>2,4,22</sup> Here, the tip is positively biased against the accelerator electrode with the acceleration voltage  $V_{ACC}$ . Another electrode between the tip and the accelerator (the extractor) is first at the same potential as the tip, and a high-purity source gas is introduced close the emission tip at a partial pressure of above  $10^{-4}$  Pa. Then, the potential of the extractor is slowly

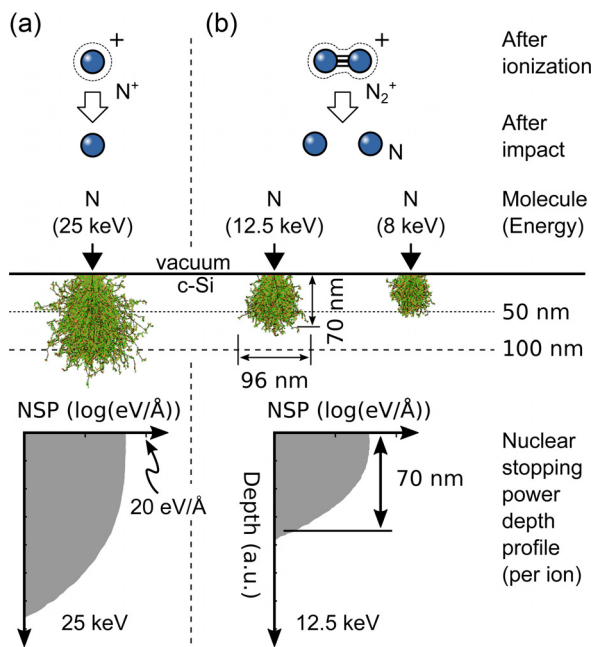


Fig. 1. (Color online) Possible ionization mechanisms of  $N_2$  gas ionized in a GFIS (Refs. 16 and 17) together with MC simulation results for 25 kV acceleration voltage: (a) The molecule splits during ionization and interacts with the sample as an atomic ion with full energy and (b) the molecule stays together during ionization but splits upon impact (modeled as N with 1/2 energy). The interaction volume and nuclear stopping power depth profiles for the two cases show the different size of the expected damage region. Additionally, the interaction volume for 16 keV acceleration voltage is shown (modeled as N with 8 keV).

decreased, forming an electric field between the tip and the extractor. Due to the shape of the tip, the field strength is largest at the tip apex. The fluctuating dipole moment of the surrounding source gas molecule and the strong electric field causes molecules that come close to the tip apex by diffusion to be transported toward the tip and transfer an electron to the tip via quantum tunneling.<sup>23</sup> The resulting ion then experiences an immediate acceleration toward the extractor and accelerator, and enters the beam column with an energy corresponding to the accelerator voltage (typically 25 keV in our system).

For milling and imaging, the beam can be positioned with a resolution of  $800 \times 800$  pixels within the field of view (FOV). The dwell time at each pixel can be controlled down to  $1 \mu\text{s}$ . A Faraday cup with a current meter is used to measure the beam current. For positioning of the milling pattern, arbitrary shapes can be drawn in the  $800 \times 800$  area or preprogrammed pattern is recalled from a database. This can be done while aligning to a previously acquired secondary electron (SE) image or on a blank canvas. The latter mode of operation was chosen here in order to avoid undesired exposure around milled lines. In this work, the FOV was fixed at  $10 \mu\text{m}$ , resulting in a distance between exposure points of 12.5 nm.

## B. Sample preparation and observation

Single crystalline silicon was used for interaction study as it is both very uniform, but also sensitive to crystal damage. A critical number of defects changes the crystalline structure into completely amorphous, allowing the visualization of the implantation depth and shape.<sup>24</sup> It has been successfully used before for investigation of numerous ion species such as helium,<sup>12</sup> neon,<sup>6</sup> and argon,<sup>24</sup> among others.

Here, we use  $\langle 100 \rangle$  crystalline silicon with the surface thoroughly cleaned from  $\text{SiO}_2$  by hydrofluoric acid etching. Next, alignment structures were patterned by electron-beam lithography [Poly(methyl methacrylate)/methyl methacrylate copolymer resist], electron evaporation of Cr/Au (6/100 nm), and consecutive lift-off in *N*-methyl-2-pyrrolidone. After solvent-based cleaning, the sample was loaded into the GFIS

microfabrication system and kept inside the main chamber during repeated ambient air evactron cleaning to ensure removal of hydrocarbon from the sample potentially remaining after the resist-based process.

For nitrogen ion beam implantation, a known position was first located on the sample via SE imaging. Consecutively, the sample was moved by a fixed offset to a location not previously exposed to the ion beam, and the line exposures were carried out. Exposure of 1 px wide lines was performed for acceleration voltages of 25 and 16 keV, respectively, and for various dwell times, resulting in line doses between 0.24 and  $9.5 \times 10^3$  ions/nm. Next, the sample was transferred to an electron beam evaporation system, and 100 nm of Ti was deposited as protective capping layer for the consecutive  $\text{Ga}^+$  FIB based TEM sample preparation.

Before FIB processing, an additional tungsten layer was deposited onto the titanium surface by ion-beam induced deposition, to avoid the specimen damage. TEM lamellae were extracted perpendicular to the milled lines by  $\text{Ga}^+$  FIB and placed on a TEM holder. The as-prepared specimens were further thinned by low-energy ion beam milling to fit for scanning transmission electron microscopy (STEM) observation. STEM observations were carried out using a spherical aberration equipped microscope ARM 200F (JEOL Co.), operated at an acceleration voltage of 200 kV. Images were taken under the high angle annular dark field (HAADF) or the annular bright field (ABF) mode.

## III. RESULTS AND DISCUSSION

### A. TEM images and subsurface damage

High resolution HAADF-STEM images taken at each milling site are given in Fig. 2. For the beam energy of 25 keV, images were acquired for a total of four different doses, ranging from 9.5 to  $0.24 \times 10^3$  ions/nm. The bright area at the top is the electron beam deposited titanium layer. Below is the silicon with the partially amorphized region. The typical bell shape of the implantation is visible in Fig. 2(a). From the cross section, the depth and width of the amorphized region can be extracted to be 70 nm in depth and 96 nm in width. A weak dent is visible

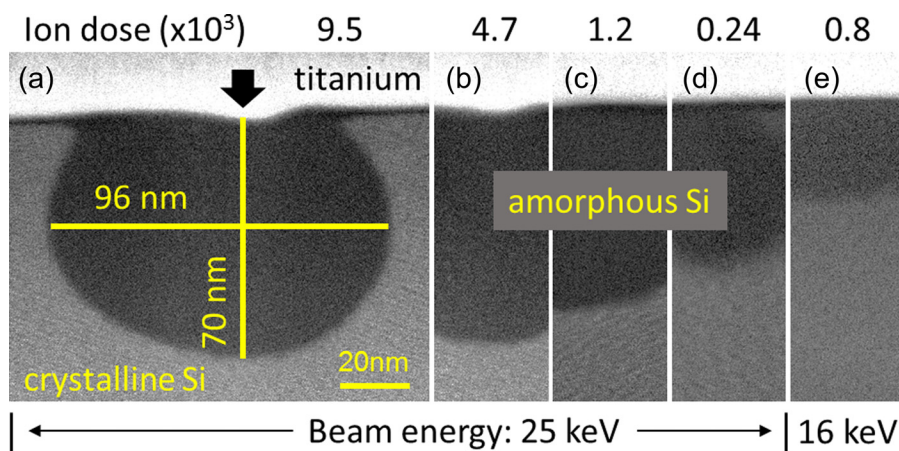


FIG. 2. (Color online) High resolution HAADF-STEM micrographs of the  $\text{N}_2^+$  bombarded area of bulk crystalline Si for 25 keV beam energy at doses of (a)  $9.5$  to (d)  $0.24 \times 10^3$  ions/nm, and (e) 16 keV at  $0.8 \times 10^3$  ions/nm. Note that the area dose in (e) is considerably lower as the beam was poorly focused during irradiation. An interface between amorphous and crystalline Si is found at  $\sim 25$  nm. Scale bar is the same for all images.

at the point where the center of the ion beam was located and a slight swelling is visible next to it. The dent is due to shrinkage or sputtering, while the latter occurs due to the increased volume of slightly amorphized Si compared to the densely packed crystal structure. The amorphized region is not symmetric, which can be caused by astigmatism or a not perfectly focused beam. Nevertheless, the extracted dimensions can be compared to the MC simulation results in Figs. 1(a) and 1(b). It is clear that the predicted implantation depth of more than 100 nm for the case of  $N^+$  [Fig. 1(a)] cannot be put into agreement with the experimental result. However, it matches the mechanism illustrated in Fig. 1(b) where the nitrogen is ionized as molecule, but breaks upon impact and interacts with the sample as two nitrogen atoms with half the energy.

With decreasing dose, the depth of the amorphous–crystalline transition zone becomes shallower as visible in Figs. 2(a)–2(d). This trend is similar to the previously reported results for  $He^+$  (Ref. 12) and  $Ga^+$  ions.<sup>11</sup> Furthermore, we obtained a cross section TEM image for a beam energy of 16 keV [Fig. 2(e)] at a dose of  $0.8 \times 10^3$  ions/nm. However, due to improper focus, the dose values cannot be directly compared with the 25 keV results as it was distributed over a larger area. Nevertheless, a clear decrease in implantation depth is observed. The transition region is at a depth of  $\sim 25$  nm.

Another important aspect of using ion beams for prototyping is the subsurface damage created when used to mill away materials above sensitive devices, such as integrated circuits. In particular, helium ions have been shown to create blisterlike defects deep below the surface,<sup>7</sup> thus making them unsuitable for some applications. Additionally, disruptions to the crystal structure below the fully amorphized region have to be considered. For this purpose, we observed the transition region for the profile in Fig. 2(a) at higher magnification, as shown in Fig. 3(a). The crystalline structure of the silicon at the bottom is visible, while a uniformly amorphized area is seen at top. Additionally, slight

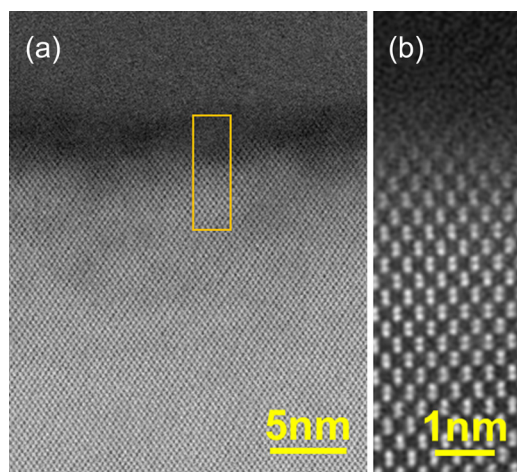


FIG. 3. (Color online) (a) High resolution ABF-STEM micrograph of the transition region from crystalline to amorphous Si for the implantation shown in Fig. 2(a). Although some amorphization is observed up to 10 nm away from the amorphous region, the well defined transition is visible. (b) Atomic resolution HAADF-STEM image of the area indicated by the rectangle in (a), which shows the dumbbell structure of Si(110).

disruptions to the silicon crystal structure can be seen up to  $\sim 10$  nm below the transition region, signified by the slight darkening in the ABF-STEM image. By zooming in further to the transition region [Fig. 3(b)], the dumbbell structure of the  $\langle 110 \rangle$  face of the Si is recognized and the sharp transition between amorphous and crystalline Si of only a few nanometer becomes obvious. These images show that the subsurface damage by the  $N_2^+$  ion beam is well confined to the fully amorphized region with a sharp transition.

Finally, we address the purity of the generated nitrogen ion beam. As has been shown by comparison of MC simulation results and experimental profiles of the subsurface damage, nitrogen gas ionized by a GFIS interacts with the silicon sample the same way a nitrogen atom with half the original energy interacts. A mechanism was proposed in Fig. 1(b) that explains this. Nevertheless, it is not guaranteed that all ionized ions are of the same kind, and it is possible that a small fraction follows a different mechanism. Therefore, we investigated the area within a range of several hundreds of nanometers right and left of the irradiated areas shown in Fig. 2, to see if there are any additional areas of sample damage. However, we were not able to identify any crystal disruptions, strongly suggesting that, for the given configuration of ion source and column, no other ions reach the sample surface. For confirmation, it would be necessary to analyze the beam by a mass spectrometer, but this is outside of the scope of this work.

## B. Molecular dynamics simulation

The experimental results discussed so far show that the nitrogen is ionized as molecule, and it is expected that the nitrogen bond is broken upon interaction with the target. To confirm this behavior and investigate the depth at which the splitting occurs, MD *ab initio* simulations were performed using *OpenMX* code which was implemented in the framework of density functional theory.<sup>25,26</sup> Such simulations had been used previously to investigate the impact of accelerated atoms onto a target.<sup>27,28</sup> All calculations are performed by using generalized gradient approximation Perdew-Burke-Ernzerhof version of the exchange-correlation potential.<sup>29</sup> In the case of for N and Si atoms, two primitive orbitals for s and p orbitals and one primitive orbital for d orbital are used. Two primitive orbitals for each s and p orbitals are used H atoms in these calculation. Here, a silicon slab consisting of 216 Si atoms was used as target (shown in Fig. 4). The slab with cubic shape has 1.63 nm extends in all directions. Hydrogen termination is used at the top and bottom surface, and the cell is periodically repeated in the  $xz$  plane (corresponding to the  $\langle 100 \rangle$  crystal plane). This relatively small slab was chosen as an appropriate trade-off between computational cost and accuracy after evaluating larger structures, as well. The  $N_2$  (nitrogen distance  $d = d_0 = 0.11$  nm) is initially positioned with a sufficient distance above the middle of the cell, and given a starting velocity in  $-y$  direction corresponding to different beam energies. The nitrogen bond is positioned directly above a Si atom. Note that it is not possible with current MD algorithms to consider electric charge (i.e., ions); however, ignoring such additional charge is acceptable as such charge is

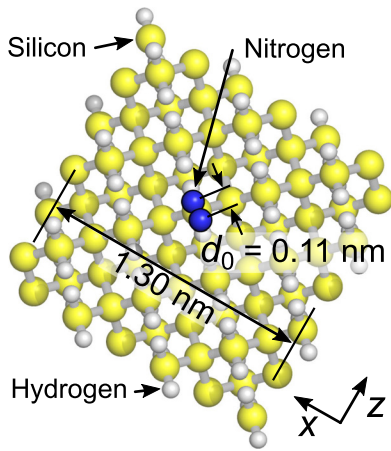


FIG. 4. (Color online) Atomic configuration of molecular dynamics simulation model. The cell with 216 silicon atoms and hydrogen termination on top and bottom is periodically repeated. The nitrogen molecule is positioned with the bond above one silicon atom and is accelerated perpendicularly toward the  $xz$ -plane ( $(100)$  crystal face).

neutralized on the surface by charge exchange.<sup>27,28,30</sup> The system is then run under a condition where the number of particles  $N$ , volume of the cell  $V$ , and total energy  $E$  are kept constant. The initial velocities of the Si and H atoms in the slab are set to 0 m/s, but are not restricted during simulation. The timestep in our simulation is set at 0.5 fs.

In Fig. 5, the atomic structure is shown for corresponding beam energies of 1 keV and 100 eV, respectively, at different simulation times. As can be seen for 1 keV in Fig. 5(a), the

distance between the nitrogen atoms increases significantly within less than 1 nm of the surface. The nitrogen atoms then continue their path through the silicon independently. For the case of 100 eV [see Fig. 5(b)], the nitrogen is separated within the first two atomic layers. Furthermore, a stronger disorder of the silicon crystal is found. This is understood as a consequence of the lower velocity and thus the longer time the atoms have to interact. At low beam energies, most of the energy is deposited at the surface, while for larger energies it is distributed over a larger depth.

With these MD simulation results, we can confirm the experimental findings reported so far: Ionization and sample interaction of nitrogen gas from a GFIS follows the mechanism illustrated in Fig. 1(b).

### C. Comparison of $N_2^+$ GFIS-FIB with other ion species

It is common practice to compare different ion species at fixed energy to get a quick grasp of what kind of beam–sample interaction is to be expected.<sup>31</sup> So far, however,  $N_2^+$  has not been included in such comparisons, partly due to the uncertainty about the molecular configuration. However, with the experimental and MD results presented so far, we can now directly compare the nitrogen ion beam at 25 keV with other common species as shown in the MC results in Fig. 6. The nitrogen molecule splits upon impact with the sample and proceeds as two atomic nitrogen with shared total energy. Thus, in the comparison in Fig. 6, all the atomic ion species ( $Ga^+$ ,  $Ar^+$ ,  $Ne^+$ ,  $Be^+$ ,  $He^+$ , and  $H^+$ ) have an

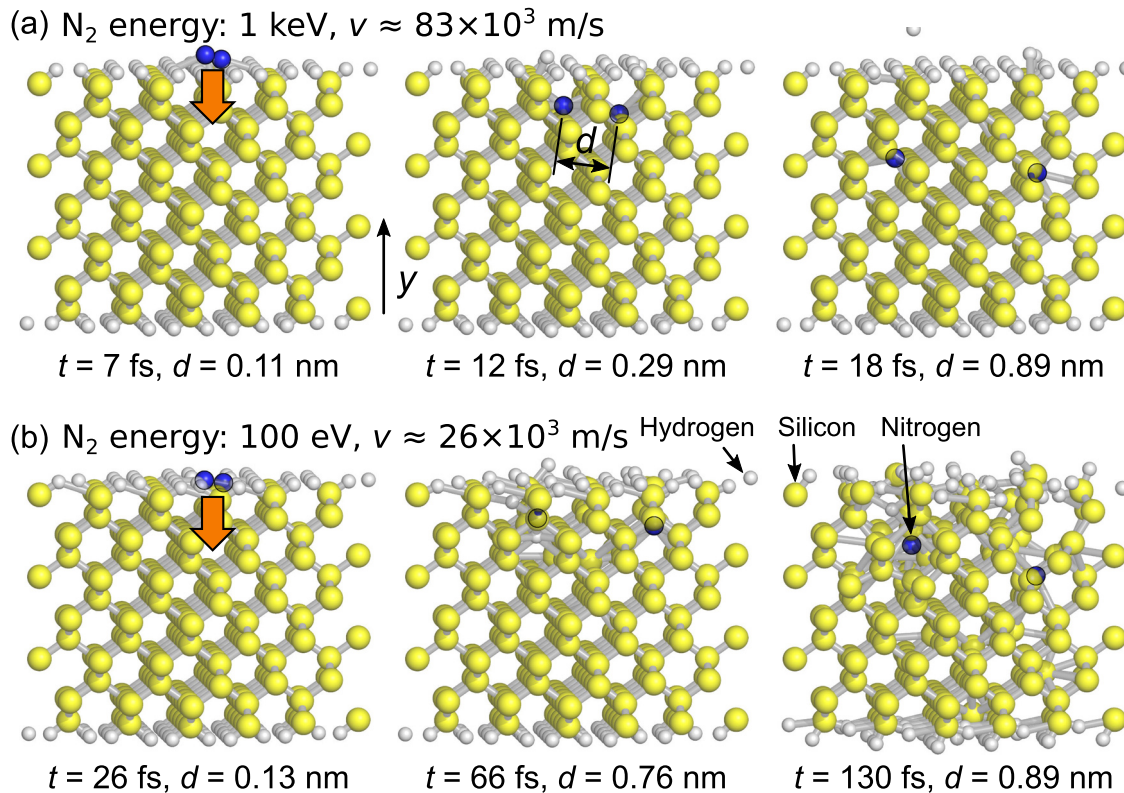


FIG. 5. (Color online) Molecular dynamics simulation results for  $N_2$  impinging on silicon with total energy of (a) 1 keV and (b) 100 eV. The resulting crystal structure is shown after impact and after different time steps. The nitrogen–nitrogen distance  $d$  is steadily increasing beyond the initial  $d_0 = 0.11$  nm, indicating that the bond is broken. In case of lower energy, a stronger disorder is found within few layers below the bombarded surface.

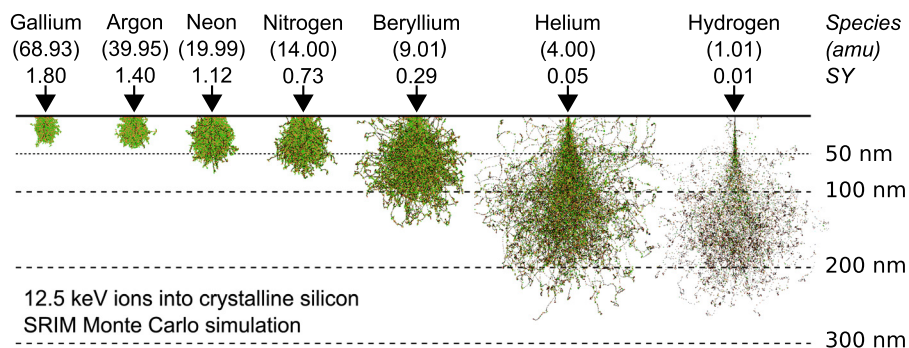


Fig. 6. (Color online) Comparison of interaction volume and sputter yield for Ga, Ar, Ne, N, Be, He, and H for corresponding ion energies of 12.5 keV.

energy of 12.5 keV. This is also the case for the atomic nitrogen; however, such a beam can only be generated by an acceleration voltage of 25 kV. Similarly, if this comparison was to be done at the same total beam energy, the energy of the nitrogen for the MC simulation has to be halved. Finally, sputter yield values are listed in Fig. 6 for the different ion species as obtained from TRIM. In contrast to the atomic ions, where this value can be directly taken, it has to be multiplied by a factor of two for the case of nitrogen. Likely, when discussing SE emission, this double number of projectiles with half energy has to be considered.

#### IV. CONCLUSION

In this work, the ionization mechanism and behavior upon sample impact has been experimentally investigated for nitrogen gas ionized in a GFIS based nanofabrication system. Based on cross-sectional STEM images of irradiated silicon samples by 25 and 16 keV beams, it is shown that the nitrogen molecule is ionized as such, but splits upon sample impact. The resulting nitrogen atoms interact with the sample independently with half of the original beam energy. Additionally, we perform MD simulations of a nitrogen molecule impinging onto the  $\langle 100 \rangle$  surface of a silicon structure. The results support the previous findings and shows that the nitrogen splits within few atomic layers. High-resolution STEM images of the transition region between amorphous and crystalline silicon show a layer of  $\sim 10$  nm with weak disruptions to the crystal lattice. Furthermore, the transition from amorphous to crystalline has a very sharp depth profile of a few nanometer.

These results clarify the nature of the  $N_2^+$  ion beam generated by the GFIS and eliminate some previous uncertainties. We explain what has to be considered when comparing the nitrogen molecular ion beam with other atomic ion beams. In particular, for  $N_2^+$ , the interaction is the same as atomic nitrogen with half of the beam energy. Additionally, the sputter and SE yield should be doubled.

The results, in particular, the localized interaction volume, indicates that the  $N_2^+$  beam is very pure, i.e., there are no alternative molecular configurations reaching the sample surface as has been reported for other ions. Analyzing the ion beam with a mass spectrometer would help to confirm this point.

#### ACKNOWLEDGMENTS

The help of M. Uno with the usage of the GFIS-FIB is acknowledged. The authors thank M. Ito for the help with TEM cross section preparation. This work was supported by the Center of Innovation (COI) program of the Japan Science Technology Agency.

- <sup>1</sup>R. H. Livengood, P. Winer, and V. R. Rao, *J. Vac. Sci. Technol. B* **17**, 40 (1999).
- <sup>2</sup>F. Aramaki, T. Kozakai, O. Matsuda, O. Takaoka, Y. Sugiyama, H. Oba, K. Aita, and A. Yasaka, *Proc. SPIE* **8441**, 84410D (2012).
- <sup>3</sup>B. W. Ward, J. A. Notte, and N. P. Economou, *J. Vac. Sci. Technol. B* **24**, 2871 (2006).
- <sup>4</sup>F. Aramaki *et al.*, *Proc. SPIE* **7969**, 79691C (2011).
- <sup>5</sup>F. H. M. Rahman, S. McVey, L. Farkas, J. A. Notte, S. Tan, and R. H. Livengood, *Scanning* **34**, 129 (2012).
- <sup>6</sup>R. H. Livengood, S. Tan, R. Hallstein, J. Notte, S. McVey, and F. H. M. Faridur Rahman, *Nucl. Instrum. Methods A* **645**, 136 (2011).
- <sup>7</sup>R. Livengood, S. Tan, Y. Greenzweig, J. Notte, and S. McVey, *J. Vac. Sci. Technol. B* **27**, 3244 (2009).
- <sup>8</sup>J. R. Rabeau *et al.*, *Appl. Phys. Lett.* **88**, 023113 (2006).
- <sup>9</sup>L. Childress and R. Hanson, *MRS Bull.* **38**, 134 (2013).
- <sup>10</sup>J. F. Ziegler, M. D. Ziegler, and J. P. Biersack, *Nucl. Instrum. Methods B* **268**, 1818 (2010).
- <sup>11</sup>S. Tan, R. Livengood, Y. Greenzweig, Y. Drezner, and D. Shima, *J. Vac. Sci. Technol. B* **30**, 06F606 (2012).
- <sup>12</sup>S. Tan, K. Klein, D. Shima, R. Livengood, E. Mutunga, and A. Vladár, *J. Vac. Sci. Technol. B* **32**, 06FA01 (2014).
- <sup>13</sup>R. H. Livengood, M. Grumski, Y. Greenzweig, T. Liang, R. Jamison, and Q. Xie, *Phys. Proc.* **1**, 143 (2008).
- <sup>14</sup>L. Pelaz, L. A. Marqués, and J. Barbolla, *Jpn. J. Appl. Phys.* **96**, 5947 (2004).
- <sup>15</sup>S. Matsubara, H. Shichi, Y. Kawanami, and T. Hashizume, *Microsc. Microanal.* **22**, 614 (2016).
- <sup>16</sup>S. Stein, *2014 Mass Spectra*, edited by P. Linstrom and W. Mallard (NIST Chemistry WebBook, Gaithersburg MD, 2016).
- <sup>17</sup>A. N. Zavilopulo, F. F. Chipev, and O. B. Shpenik, *Tech. Phys.* **50**, 402 (2005).
- <sup>18</sup>R. Ramachandra, B. Griffin, and D. Joy, *Ultramicroscopy* **109**, 748 (2009).
- <sup>19</sup>SRIM, Using *detailed calculation with full damage cascade* for damage simulation. Target is Si with 28.089 amu and 2.32 g/cm<sup>2</sup>, 2008.
- <sup>20</sup>K. Dobes, M. Köppen, M. Oberkofler, C. P. Lungu, C. Porosnicu, T. Höschen, G. Meisl, C. Linsmeier, and F. Aumayr, *Nucl. Instrum. Method B* **340**, 34 (2014).
- <sup>21</sup>A. D. Yadav and M. C. Joshi, *Thin Solid Films* **59**, 313 (1979).
- <sup>22</sup>F. Aramaki, T. Kozakai, O. Matsuda, A. Yasaka, S. Yoshikawa, K. Kanno, H. Miyashita, and N. Hayashi, *Proc. SPIE* **9235**, 92350F (2014).
- <sup>23</sup>E. W. Müller and K. Bahadur, *Phys. Rev.* **102**, 624 (1956).
- <sup>24</sup>A. Claverie, C. Vieu, J. Fauré, and J. Beauvillain, *Jpn. J. Appl. Phys.* **64**, 4415 (1988).
- <sup>25</sup>T. Ozaki, *Phys. Rev. B* **67**, 155108 (2003).
- <sup>26</sup>“OpenMX,” <http://www.openmx-square.org/>.

- <sup>27</sup>O. Lehtinen, J. Kotakoski, A. V. Krasheninnikov, A. Tolvanen, K. Nordlund, and J. Keinonen, *Phys. Rev. B* **81**, 153401 (2010).
- <sup>28</sup>E. P. Bellido and J. M. Seminario, *J. Phys. Chem. C* **116**, 4044 (2012).
- <sup>29</sup>J. P. Perdew, K. Burke, and M. Ernzerhof, *Phys. Rev. Lett.* **77**, 3865 (1996).
- <sup>30</sup>A. Ito, H. Nakamura, and A. Takayama, *J. Phys. Soc. Jpn.* **77**, 114602 (2008).
- <sup>31</sup>S. Tan, R. Livengood, D. Shima, J. Notte, and S. McVey, *J. Vac. Sci. Technol. B* **28**, C6F15 (2010).